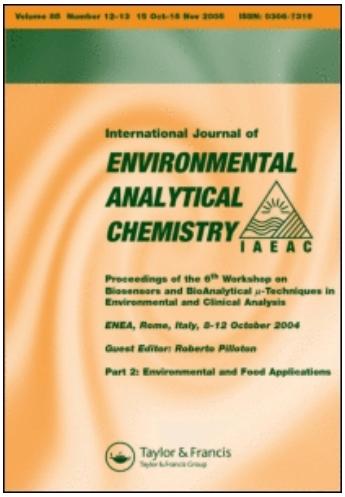

International Journal of Environmental Analytical Chemistry

Publication details, including instructions for authors and subscription information:
http://www.informaworld.com/smpp/title~content=t713640455

Radioactive disequilibrium and geochemical modelling as evidence of uranium leaching from gold tailings dumps in the Witwatersrand Basin

Hlanganani Tutu[a]; Ewa M. Cukrowska[a]; Terence S. McCarthy[b]; Roger Hart[c]; Luke Chimuka[a]
[a] School of Chemistry, South Africa [b] School of Geosciences, University of the Witwatersrand, South Africa [c] iThemba LABS (Gauteng), WITS 2050, South Africa

Online publication date: 22 September 2010

To cite this Article Tutu, Hlanganani , Cukrowska, Ewa M. , McCarthy, Terence S. , Hart, Roger and Chimuka, Luke(2009) 'Radioactive disequilibrium and geochemical modelling as evidence of uranium leaching from gold tailings dumps in the Witwatersrand Basin', International Journal of Environmental Analytical Chemistry, 89: 8, 687 — 703
To link to this Article: DOI: 10.1080/03067310902968749
URL: http://dx.doi.org/10.1080/03067310902968749

Intern. J. Environ. Anal. Chem.
Vol. 89, Nos. 8–12, 15 July–15 October 2009, 687–703

Taylor & Francis
Taylor & Francis Group

Radioactive disequilibrium and geochemical modelling as evidence of uranium leaching from gold tailings dumps in the Witwatersrand Basin

Hlanganani Tutu[a]*, Ewa M. Cukrowska[a], Terence S. McCarthy[b], Roger Hart[c] and Luke Chimuka[a]

[a]*School of Chemistry;* [b]*School of Geosciences, University of the Witwatersrand, South Africa;* [c]*iThemba LABS (Gauteng), P. Bag 11, WITS 2050, South Africa*

(*Received 9 September 2008; final version received 24 March 2009*)

Gold tailings dams from the Witwatersrand Basin usually contain elevated amounts of heavy metals and radionuclides. Uranium, in the form of uraninite (UO_2) and brannerite (UTi_2O_6), is normally associated with gold-bearing ores in the basin. As a result of acid mine drainage (AMD), uranium is released into groundwater and fluvial systems. Its transport, retardation and immobilisation depend strongly on the uranium species and prevailing geochemical conditions. This study was aimed at the quantitative assessment of the distribution of uranium based on measurement of its radioactivity and modelling of its geochemical speciation. Analyses of tailings, water and sediment in areas of previous mining were performed. The results indicate that there is active leaching of uranium from the tailings, transport of soluble uranium species through water systems, with subsequent deposition of insoluble uranium species in sediments of fluvial systems. Analysis of tailings material indicated that mobilisation and transportation of uranium from the tailings resulted in its decoupling from its progeny which remained largely unaffected by the weathering effects. Mobilisation occurs as uranium is oxidised to the U(VI) state which dominates aqueous chemistry, particularly via complexation with most ligands. The U(VI) is reduced to U(IV) which is immobile and is subsequently deposited in the wetland sediments downstream from the primary acid mine drainage. Geochemical modelling of uranium speciation revealed the two most influential hydrogeochemical facies in uranium mobility, namely a sulphate-dominated AMD system and a lime-neutralised carbonate-dominated system. In both cases, the uranium was shown to be soluble throughout a very wide pH regime, thus yielding important information for risk assessment considerations.

Keywords: radioactive disequilibrium; Witwatersrand Basin; geochemical modelling

1. Introduction

Uranium has been an important by-product of gold mining. It occurs with gold and a host of other minerals in the Witwatersrand Basin (Figure 1) and can be at elevated concentrations of between 100 and 300 $\mu g\,g^{-1}$ [1]. Since the decline in its production in the 1980s, uranium has largely been discarded in gold tailings [2]. An increase in demand for

*Corresponding author. Email: hlanganani.tutu@wits.ac.za

ISSN 0306–7319 print/ISSN 1029–0397 online

DOI: 10.1080/03067310902968749
http://www.informaworld.com

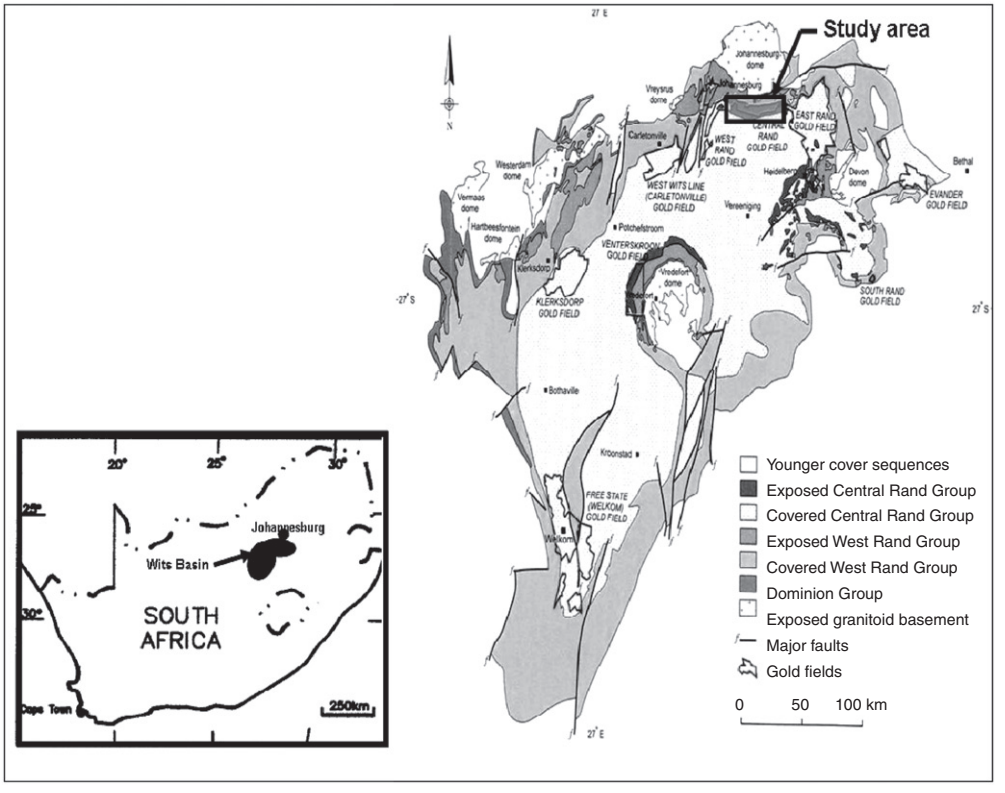

Figure 1. Geological map of the Witwatersrand showing the locations of its major goldfields.

alternative and cleaner sources of fuel than fossil fuels has encouraged a series of exploration projects in the Witwatersrand Basin and the establishment of a number of uranium mines [3].

With slimes dams in the goldfields of the Witwatersrand Basin covering an area of about 400 km^2 and containing some 430,000 tons of U_3O_8, they constitute an environmental problem of extraordinary spatial dimensions [4]. Effects range from water pollution (the result of acid mine drainage (AMD) generated mainly from sulphides in the tailings dams), and air pollution in the form of airborne dust from unrehabilitated or partially rehabilitated and reprocessed tailings dams [5].

Natural uranium consists of three isotopes, namely, U-234 (0.0054%), U-235 (0.72%) and U-238 (99.2746%). The nuclides in the U-238 decay chain mainly decay by α and β emission. γ emission is significantly pronounced in cases such as Bi-214 and Pb-214 where the products of β emission are left in one of several excited states and decay by the release of strong γ radiation (typically 1.76 MeV) [6,7]. Thorium-232 also decays by a sequence of α and β emissions with a stable non-radioactive Pb-208 being the end product [8].

In a closed system, there are no losses or gains of any decay chain members. In such a system, the activities of all products in the decay chain are equal and their ratio is unity. The chain members are said to be in radioactive equilibrium. In the natural environment, radioactive disequilibrium occurs as a result of disturbances by physical and/or chemical

processes that enhance a loss or gain of a certain decay product [9]. These processes include weathering, erosion, sedimentation, precipitation, dissolution, and crystallisation among others.

Radioactive disequilibrium in the U decay series has been studied in a number of different environmental systems [7,10–12].

While a number of studies on uranium pollution in the Witwatersrand goldfields have been carried out [2,4,13,14], only a few of them have focused on measurements of radioactivity.

Significant radiometric anomalies were detected during airborne radiometric mapping surveys over mining sites in the East Rand area. The radiometric studies [15–17] revealed that high gamma-activities emanating from immobile daughters such as ^{226}Ra of the uranium decay series in tailings dams pose a serious threat to the nearby environment as a result of dust dispersion. Funke [18] highlighted that radioactivity measurements had pointed to high Ra-226 concentrations in mine effluents and in some surface streams.

In this paper, the aim is to assess radioactive anomalies in both U-238 and Th-232 decay chains in tailings and wetland sediments in a mining area. The possible reasons for these anomalies and underlying mechanisms for the observed effects are discussed. Geochemical modelling has been used in order to simulate the processes affecting radioactive disequilibrium and its relevance for uranium mobility.

2. The study area

The study area covers the Central Rand Goldfield of the Witwatersrand Basin (Figure 2) and is characterised by a well-defined drainage system including streams and wetlands which form the tributaries of the upper Klip River, in turn a tributary of the Vaal River from which Johannesburg obtains the bulk of its water supply. Extensive wetlands are developed along the course of the Klip River as well as at the mouths of streams discharging into many of the dams in the area. The streams in the study area are of importance since they drain the reef outcrop, areas of tailings dams, light industrial areas and old mine workings, which serve as sources of pollution.

Previous studies by the authors [19,20] have enabled the development of a conceptual model of the generation and dispersal of mining-related pollution in the study area. The model contextualises the sampling strategy and the results obtained in this study as well. The area was summarised into sub-components, namely: dumps which are the main source of pollution; streams which include streams flowing through tailings footprints and reprocessing areas, distributaries and natural streams near or distal to pollution sources; wetlands which are common along the streams and rivers in the mining areas, and are vegetated mainly by *Phragmites* and *Typha* spp. reeds; and dams which tend to trap sediment (including tailings) eroded from the upstream catchment. Groundwater sources, depicted to be leachates from the dumps as well as from residential areas, contribute to the base flow of streams and recharge to dams [19,20].

3. Experimental

3.1 *Sampling procedure*

Wetland sediments and tailings samples were collected (using an auger), dried and sieved to <2 mm. These were collected in April 2004 at Sites SJ and B (see Figure 2) and

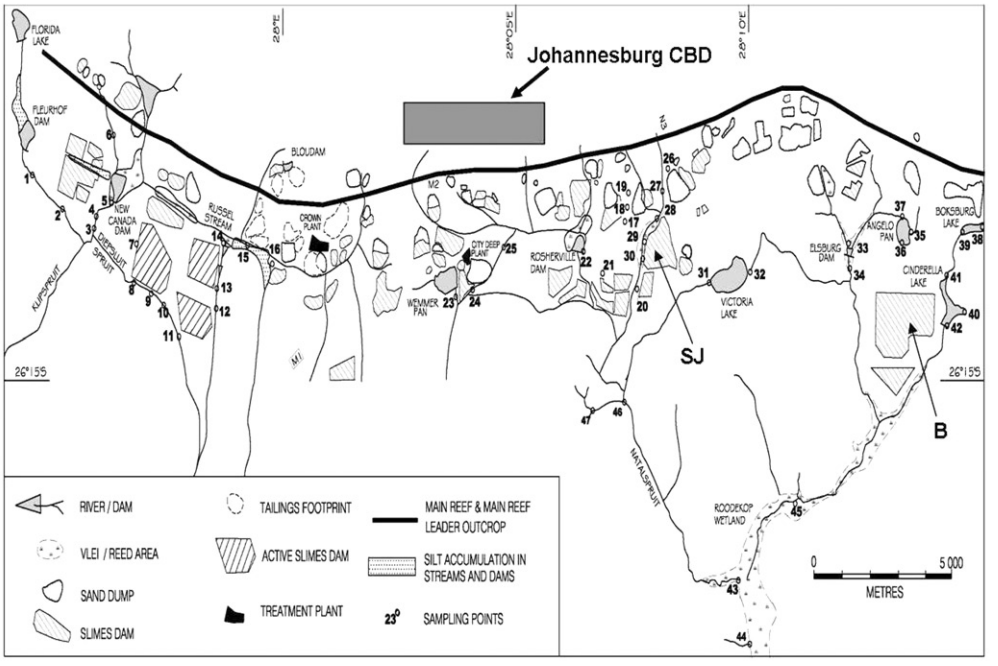

Figure 2. Map of the central portion of the Central Rand goldfield showing the locations of tailings deposits and related features, and the location of sampling sites.

a detailed description is given in Table 1. One portion of each of the samples was digested (using *aqua regia* and hydrofluoric acid) in a microwave and a second portion was stored for two weeks prior to measurement of radioactivity. Some of the tailings samples were sent for iron analysis.

A series of surface water samples were also collected at the various sources mentioned above. The sampling points are shown in Figure 2 as numbered points. The water samples were collected and stored according to commonly accepted sampling procedures [21]. Groundwater samples were collected at some sites adjacent to surface water sites by making auger holes that intercepted the water table. The samples were collected in acid-washed and conditioned one-litre polypropylene (PP) bottles. The samples were filtered (0.45 μm cellulose acetate filter) using a vacuum pump. Samples for metal analysis were acidified to pH <2 with concentrated HNO_3 and stored in the refrigerator at 4°C pending analysis while those for anion analysis were only filtered and analysed immediately.

3.2 *Analytical methods*

An ORTEC gamma spectrometer multi channel analyser (MCA) with 8192 channels was used for measurement of radioactivity. The High Purity Ge n-type nitrogen cooled detector with a relative efficiency of 36% was used. The software used was the Genie 2000 Basic Spectroscopy Software. The software included a set of basic spectroscopic analysis algorithms which are essential for locating spectral peaks and calculating peak net areas. U-238 was determined by the γ-rays of Ra-226 after allowing for equilibrium between Ra-226 and U-238 to be reached, that is, after two weeks of storage [6]. The Bi-214 isotope

Table 1. Description of the tailings and wetland sediments.

Sample	Depth	Description
Tailings		
SJT1	0–40 cm	Orange-brown, dry
SJT2	40–80 cm	Orange-brown, moist
SJT3	80–120 cm	Orange-brown, moist
BT1	0–40 cm	Orange-brown, dry
BT2	40–80 cm	Orange-brown, moist
BT3	80–120 cm	Greyish, moist
BT4	120–200 cm	Greyish, moist
Wetland sediments		
SJW1	0–40 cm	Brownish, wet
SJW2	40–80 cm	Greyish to black, high portions of organic matter, wet
SJW3	0–40 cm	Brownish, plant remains, wet
SJW4	40–80 cm	Dark brown to greyish, plant remains, wet
SJW5	0–40 cm	Dark brown to greyish, plant remains, wet
BW1	0–40 cm	Dark brown, plant remains, wet
BW2	40–80 cm	Greyish to black, high portions of organic matter, wet
BW3	0–40 cm	Dark brown, plant remains, wet

with an energy output of 609.3 keV and Ac-228 isotope with an energy output of 911.2 keV were used for U-238 and Th-232 determination, respectively [22]. Analytical reference materials of comparable density for U_3O_8 and ThO_2 were obtained from IAEA (International Atomic Energy Agency, Vienna, Austria).

Five hundred grams of standards and samples were weighed and filled into Marinelli beakers which were then placed on the detector. Background correction was done and counts were recorded after 2 hours (in relation to the detector efficiency). Lead blocks were used to make the outer casing so as to reduce background radiation.

Iron redox speciation in the tailings was analysed by Mössbauer-effect spectroscopy at the School of Physics at the University of the Witwatersrand.

The concentrations of metals in water and digested solid samples were determined using a Spectro Ciros Inductively Coupled Plasma Optical Emission Spectroscopy (ICP OES) with coupled charge detection (CCD) (Spectro, Germany). Sulphates and other important anions were determined using the Metrohm 761 Compact Ion Chromatograph with a Metrosep A Supp 5 (6.1006.520) 150 × 4.0 mm analytical column. All solutions were prepared with purified water obtained by passing distilled water through a Milli-Q-water purification system. Bicarbonates were analysed by titration with acid according to standard methods [23]. Blank samples consisting of purified, deionised water were used to assess the level of contamination due to the analytical procedures used for this study and to quantify any background concentrations. All chemicals were of analytical grade obtained from Aldrich, Industrial Analytical and Merck. Standards for γ-spectroscopy were obtained from the International Atomic Energy Agency (Vienna, Austria).

The geochemical parameters were recorded using a Universal Multi-line P4-SET3 field meter (WTW, Germany) equipped with pH combined electrode with integrated temperature probe (SenTix 41), standard conductivity cell (Tetra Con 375) and

oxidation-reduction potential probe (SenTix ORP). The pH electrode was calibrated according to the International Union of Pure and Applied Chemistry (IUPAC) recommendations against two buffer solutions at pH 4 and pH 7. Redox potentials were obtained from platinum vs Ag/AgCl electrodes. The electrodes were checked by a standard buffer solution. All potentials reported were corrected relative to the standard hydrogen electrode (SHE). An uncertainty of about ± 0.1 units ($1\,\sigma$) is assumed for pH and an uncertainty of ± 30 mV is assumed for Eh, corresponding to the average fluctuation observed during field sampling. The conductivity error is about $\pm 0.002\,\mathrm{mS\,cm^{-1}}$.

The analytical results for water samples (geochemical parameters, metal and anion concentrations) were used for modelling the speciation of uranium. Modelling was done using the Act2 module of the Geochemist's Workbench release 4.0 software (Rockware, USA). The thermodynamic database used was the thermo.dat. From the geochemical parameters and total component concentrations (entered as log activities), the software established equilibria accounting for precipitation and dissolution of species. Sites depicting similar chemical composition were grouped together and modelled as composite samples.

4. Results and discussion

4.1 *Measurements of radioactivity*

The results for uranium concentrations found in tailings and wetland sediments are presented in Figure 3. The results depict a comparison of analysis by ICP-OES and γ-spectroscopy on the same samples.

Discrepancies between the two methods of analysis can be observed. In tailings (Figure 3a), higher concentrations are obtained by γ-spectroscopy compared to ICP-OES and vice versa for the wetland sediments (Figure 3b). The discrepancies can be explained by the phenomenon of radioactive disequilibria. In the tailings, uranium is decoupled from its progeny owing to AMD as U-238 is more soluble compared to Bi-214 and Pb-214. ICP techniques determine uranium more accurately whereas γ-spectroscopy determines uranium indirectly from Bi-214 or Pb-214. Notwithstanding that in wetland sediments the leaching is much less in total than in the tailings, the uranium accumulating there is generally not accompanied by its progeny. This results in low counts on the γ-spectrometer. On close inspection, it can be noted that for the samples collected at B the upper two samples (BT1 and BT2) display significant discrepancies between the two techniques whereas the lower two (BT3 and BT4) do show a discrepancy but not to a very significant extent. For instance, in BT1 (0–40 cm) the concentrations of uranium recorded are 43 and $105\,\mathrm{mg\,kg^{-1}}$ by ICP-OES and γ-spectroscopy, respectively. However, in BT3 (80–120 cm) the concentrations recorded were about 73 and $105\,\mathrm{mg\,kg^{-1}}$ by ICP-OES and γ-spectroscopy, respectively. This reflects that equilibrium is somehow being approached with depth through the tailings. The upper 50 to 100 cm in tailings (particularly slimes) are usually oxidised whereas the deeper layers are largely unoxidised [20]. The descriptions given in Table 1 further point to this. For instance, all the samples collected from SJ (SJT1-SJT3) and the samples in upper layers in B (i.e. BT1 and BT2) were observed to be orange-brown in colour (i.e. oxidised) whereas samples in lower layers (BT3 and BT4) were observed to be greyish (unoxidised). These observations prompted for investigations regarding the relationship between oxidation within tailings and radioactive disequilibrium which is discussed below.

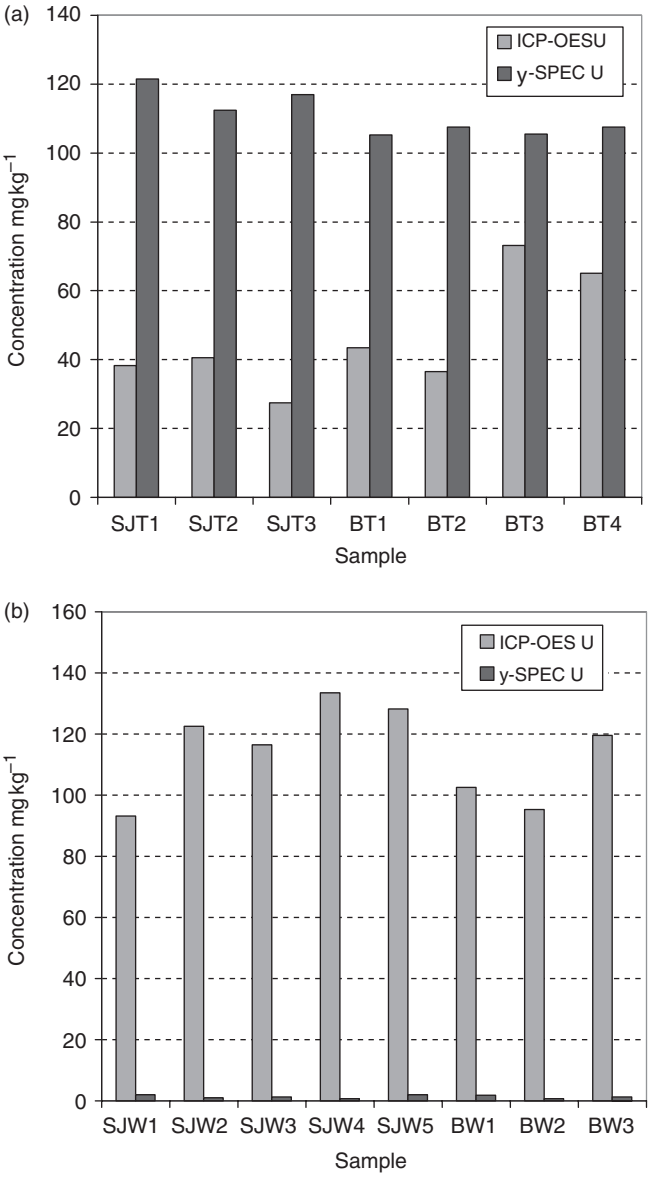

Figure 3. ICP-OES and γ-spectroscopy measurements for uranium in (a) tailings and (b) wetland sediments from SJ and B.

4.1.1 *The significance of the Fe^{2+}/Fe^{3+} redox speciation on uranium mobility*

Figure 4 presents a general summary of the pathways followed by uranium as it is released from tailings to wetlands and other aquatic systems. The observations mentioned above regarding uranium concentrations determined by ICP-OES and γ-spectroscopy in tailings and wetland sediments are also summarised in the figure. It can be observed that equilibrium is approached in the unoxidised layer of tailings. Since Fe is the major element determining redox conditions in the tailings (up to 5% pyrite is present in the ores),

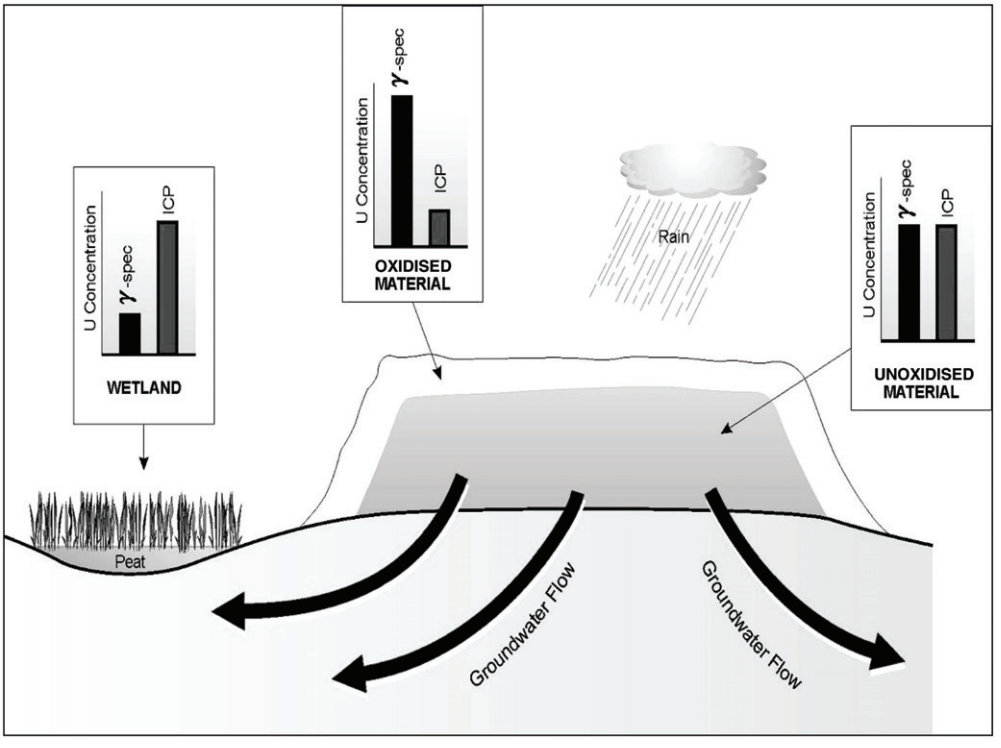

Figure 4. ICP-OES and γ-spectroscopy measurements for thorium in (a) tailings and (b) wetland sediments from SJ and B.

its redox speciation was studied. The study was done on B samples and the results are presented in Table 2. It can be observed that uranium radioactive equilibrium is approached with depth and increasing concentrations of Fe^{2+}. However, it should be noted here that further studies would be required to assess the amount of uranium leached out and that adsorbed or co-precipitated with hydrous ferric oxides.

Thorium on the other hand showed a different trend to that observed for uranium (Figure 5). There were no large discrepancies in concentrations of Th in tailings measured by the two techniques (Figure 5a). As mentioned previously, Th is measured indirectly via the Ac-228 isotope. Since there is no discrepancy, it can be concluded that Th is in

Table 2. Uranium concentrations by ICP-OES and γ-spectroscopy and iron redox concentrations.

Sample	$U_{ICP\text{-}OES}$ (mg kg^{-1})	U_{γ} (mg kg^{-1})	Fe^{2+} (%)	Fe^{3+} (%)	Fe^{2+}/Fe^{3+}
BT1	43.4	105.2	29	71	0.41
BT2	36.54	107.5	32	68	0.47
BT3	73.1	105.5	62	38	1.63
BT4	65	106.8	60	40	1.50

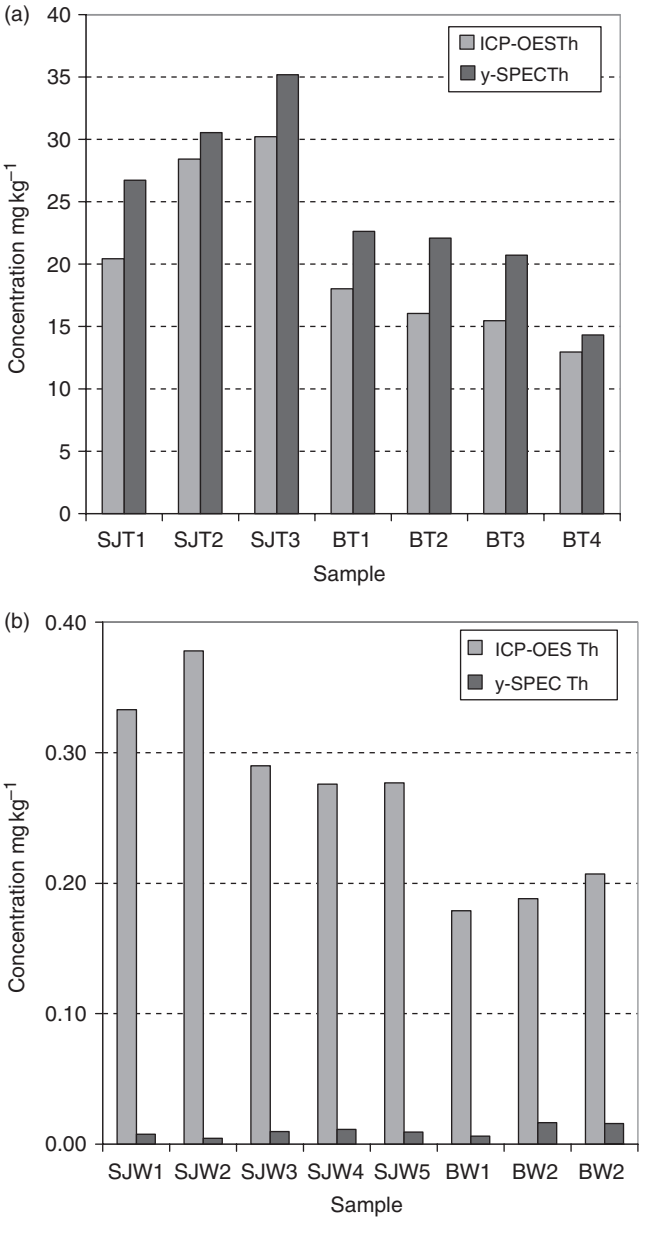

Figure 5. Sketch of a tailings dump and illustrations for uranium analysis at different locations using ICP-OES and γ-spectroscopy.

radioactive equilibrium with Ac. This is attributable to the fact that both elements are not very mobile and as such tend to accumulate in the tailings. In wetlands however, the results from ICP-OES were notably higher than for γ-spectroscopy. The magnitude of the concentrations is not very significant though compared to the case for the tailings. This substantiates the fact that Th and Ac are relatively immobile compared to uranium.

4.2 *Geochemical modelling*

The water samples presented a number of interesting chemically varying cases. The detailed analytical results for these samples are presented in Table 3 (surface water) and Table 4 (groundwater). The samples were collected from a number of sites in the gold mining region in order to assess the extent of leaching of uranium from the tailings. The groundwater samples display moderately high Eh values, that is, in the range +300 to +400 mV. This is due to the water being within less than a metre of reach from the surface, implying interaction with atmospheric oxygen. Thus the redox potentials in these samples do not reflect elevated reduction as would be expected of water from deeper zones.

The sampled sites were characterised by geochemical modelling as hydrogeochemical facies in order to understand the prevailing conditions influencing the speciation of uranium and, subsequently, its mobility. The hydrogeochemical facies studied include those that contain high sulphate concentrations (up to 1000 mg L^{-1}); very high sulphate levels (e.g. up to 7000 mg L^{-1}); and those at buffered sites (containing carbonate). Generally, these address the different chemistries of tailings and that of the water plumes draining from them. For instance, freshly deposited tailings (or active slimes), rehabilitated tailings footprints, and underground water that is treated and discharged into surface water bodies have elevated pH. Older tailings and particularly those being reworked usually have low pH within the oxidation fronts and drainage from them is of low pH and contains high concentrations of sulphate and metals [20].

Case 1 Uranium speciation in high sulphate acid mine surface water – streams

Figure 6 shows a generic Eh-pH diagram for uranium speciation in water samples collected from streams impacted by acid mine drainage with sulphate concentrations up to 1000 mg L^{-1} (see Table 3).

The dots, triangles and squares within Figure 6 represent samples from streams in the vicinity of tailings dams. The dots represent streams close to pollution sources while the triangles represent samples mid-way within the group and still fairly close to pollution sources. The squares represent samples collected away from the pollution sources, but still sufficiently influenced by AMD. The darker shade shows the soluble phases while the lighter shade shows the solid phases. The model predicts that uranium will exist as soluble uranyl sulphate (UO_2SO_4(aq)) in all but one sample. The samples farther from the pollution sources tend to undergo dilution and neutralisation, thus an increase in pH can be noted. The trend in the data approaches the pH of hydrolysis for uranium and is signified by the formation of schoepite (a uranyl hydroxide solid phase) within Figure 6.

Case 2 Uranium speciation in very high sulphate acid mine water – groundwater and severely impacted streams draining from tailings footprints and trenches

Figure 7 shows a generic Eh-pH diagram for uranium speciation in samples collected from waters severely impacted by acid mine drainage with sulphate concentration up to 7000 mg L^{-1} (see Tables 3 and 4). The samples from these extremely polluted environments were modelled as a group.

The model predicts that uranium in the samples will exist mainly as the solid uranyl sulphate ($UO_2SO_4{\cdot}3H_2O$) complex. This is not unexpected as the samples were observed to be highly saturated. By assuming equilibrium in the system components, the model determines the stable mineral assemblage and corresponding fluid composition. The supersaturated minerals are allowed to precipitate, and then accounting for any minerals

Table 3. Geochemical parameters and chemical composition of surface water samples.

				Field parameters			Major anions			Major cations				Trace elements							
		Location					($mg\,L^{-1}$)			$mg\,L^{-1}$				$mg\,L^{-1}$							
Sample No.	Description	E	S	pH	Eh (mV)	EC ($mS\,cm^{-1}$)	SO_4^{2-}	NO_3^-	Cl^-	Na	K	Ca	Mg	Al	Cu	Co	Fe	Mn	Ni	Zn	U
1	Stream	27°54′37.37″	26°12′26.66″	3.5	671	2.68	988.7	3.860	61.51	84.50	25.48	141.2	47.25	20.10	0.121	2.620	6.810	68.30	1.530	0.750	3.042
2	Stream	27°55′20.28″	26°12′57.52″	6.9	450	0.78	128.6	9.940	60.41	49.70	9.44	55.80	48.90	0.157	0.025	0.090	0.119	5.550	0.125	0.030	0.700
3	Stream	27°55′59.31″	26°13′05.08″	3.8	592	1.30	515.1	8.810	4.120	37.56	12.47	129.0	46.57	0.516	0.116	0.554	2.720	4.470	1.187	0.009	0.930
4	Stream	27°56′16.47″	26°12′55.21″	3.8	610	1.30	554.8	7.560	0.120	34.54	11.54	127.9	42.20	0.562	0.157	0.573	3.130	4.450	1.208	0.009	0.870
5	Stream	27°56′20.98″	26°12′34.65″	3.5	684	1.28	510.8	5.650	6.610	35.30	10.86	132.5	43.38	0.244	0.042	0.395	0.539	4.369	0.899	0.167	0.530
6	Stream	27°55′53.11″	26°12′07.86″	6.7	422	0.69	108.9	3.520	69.02	38.64	10.28	31.83	18.69	0.030	0.025	0.027	0.050	0.008	0.125	0.014	0.158
7	Stream	27°56′53.81″	26°13′23.29″	3.7	380	4.05	1501	4.190	73.46	195.0	80.40	154.7	50.37	0.770	0.060	1.471	42.69	23.73	0.620	0.145	0.515
8	Stream	27°56′42.66″	26°13′50.37″	6.0	280	4.35	1291	8.570	90.41	170.5	83.80	133.7	53.46	0.053	0.148	0.564	252.7	32.76	0.125	0.015	0.067
9	Stream	27°56′59.27″	26°13′58.52″	4.8	304	4.04	1355	2.280	99.59	198.1	68.70	153.1	45.27	14.20	0.243	2.198	217.6	28.86	2.281	0.953	0.102
10	Stream	27°57′27.56″	26°14′06.25″	3.0	608	6.03	2395	2.310	86.98	131.7	37.35	126.0	99.80	138.9	2.948	7.77	1010	31.01	15.44	9.980	7.550
11	Stream	27°57′51.84″	26°14′47.78″	3.3	540	5.08	2350	2.180	70.74	105.5	36.45	143.6	47.40	86.20	2.340	6.190	86.10	33.04	14.21	6.570	9.820
12	Stream	27°58′28.67″	26°14′05.22″	3.3	553	9.47	3110	18.78	76.48	136.8	52.90	135.3	94.40	109.0	1.122	6.560	113.9	33.32	12.75	6.740	8.690
13	Stream	27°58′32.39″	26°13′55.88″	4.4	450	3.08	336.6	0.130	40.22	105.8	30.76	108.9	93.50	17.43	5.770	3.682	166.0	0.508	11.02	2.215	5.420
14	Stream	27°58′45.01″	26°13′23.69″	6.8	322	0.80	276.4	6.830	17.79	14.50	4.82	85.40	44.16	0.030	0.025	0.027	0.161	0.008	0.125	0.012	0.07
15	Stream	27°59′17.66″	26°13′32.00″	2.5	700	6.53	2554	6.470	97.53	132.0	71.18	202.1	44.40	430.8	0.03	37.84	269.7	118.9	71.10	107.5	23.8
16	Stream	28°00′14.13″	26°13′41.34″	4.2	469	2.60	273.8	8.880	39.65	50.50	15.26	52.97	71.70	24.70	1.352	2.107	127.0	6.260	5.490	2.094	2.700
17	Dam	28°07′53.44″	26°12′56.27″	6.5	592	0.77	325.9	4.070	7.78	24.03	8.20	63.60	9.68	0.030	0.025	0.177	0.078	4.301	0.295	0.259	0.073
18	Stream	28°07′55.26″	26°12′49.16″	4.5	590	0.93	439.6	4.550	44.08	24.54	7.77	101.2	50.50	9.540	0.294	0.524	0.694	3.384	0.969	1.394	0.196
19	Dam	28°07′45.12″	26°12′41.23″	8.7	564	0.60	252.9	5.480	29.97	36.07	6.11	82.40	12.21	0.108	0.148	0.027	0.150	0.075	0.125	0.085	0.014
20	Stream	28°07′33.12″	26°13′57.84″	2.9	710	3.01	1210	5.570	71.45	34.24	14.75	129.0	45.27	62.40	1.023	3.093	24.32	15.16	5.060	6.290	3.220
21	Dam	28°06′33.63″	26°13′51.27″	6.6	593	0.70	98.7	4.560	32.05	24.35	8.30	55.20	28.60	0.109	0.025	0.027	0.112	0.462	0.125	0.032	0.09
22	Dam	28°06′25.25″	26°13′29.49″	6.7	575	0.72	110.2	3.640	29.62	28.33	9.63	58.90	33.34	0.030	0.051	0.027	0.159	2.531	0.125	0.009	0.03
23	Dam	28°03′42.04″	26°13′56.30″	7.1	595	0.36	127.4	3.930	0.00	13.10	5.63	36.18	14.92	0.079	0.055	0.027	0.109	0.595	0.125	0.032	0.03
24	Stream	28°03′54.20″	26°14′03.80″	2.3	762	10.65	7571	3.580	99.26	151.3	81.54	334.7	139.5	629.0	11.43	17.11	113.9	62.50	42.33	91.80	72.7
25	Stream	28°04′32.62″	26°13′39.65″	3.4	604	1.45	551.5	5.150	38.40	18.89	6.010	74.50	74.80	72.20	1.990	1.680	17.52	3.260	3.531	3.634	8.710
26	Stream	28°08′08.56″	26°12′53.19″	6.8	382	0.52	163.7	4.780	21.80	22.55	6.120	53.45	20.59	27.29	2.910	1.560	26.15	0.900	6.500	0.330	0.053
27	Stream	28°08′06.54″	26°13′00.50″	6.4	311	0.72	396.1	8.380	24.30	35.49	6.150	65.90	20.55	5.090	2.910	1.640	8.260	15.33	2.150	0.500	0.042

(*Continued*)

Table 3. Continued.

Sample No.	Description	Location E	Location S	Field parameters pH	Eh (mV)	EC (mS cm^{-1})	Major anions (mg L^{-1}) SO_4^{2-}	NO_3^-	Cl^-	Major cations mg L^{-1} Na	K	Ca	Mg	Trace elements mg L^{-1} Al	Cu	Co	Fe	Mn	Ni	Zn	U
28	Stream	28°07′58.61″	26°13′07.72″	5.4	360	0.88	579.7	3.850	24.52	39.54	6.120	83.30	32.86	5.090	2.910	1.750	0.800	18.98	2.150	0.330	0.030
29	Stream	28°07′44.98″	26°13′16.94″	3.0	693	1.6	1780	4.590	75.36	71.20	6.120	102.2	48.16	9.450	2.910	0.142	22.86	33.31	2.080	7.180	0.020
30	Stream	28°07′41.07″	26°13′41.84″	3.9	605	1.4	370.5	2.370	35.48	31.73	6.120	71.90	36.09	16.38	2.910	1.650	7.960	17.97	21.50	18.08	0.040
31	Dam	28°09′08.46″	26°13′55.01″	7.4	570	0.48	507.1	0.203	9.005	27.14	10.40	89.40	41.09	0.050	0.029	0.017	0.022	0.012	0.215	0.003	0.040
32	Dam	28°09′54.52″	26°13′46.60″	7.6	594	0.54	357.0	8.245	2.960	8.11	6.120	76.57	36.12	5.090	0.015	1.560	0.800	0.440	0.087	0.001	0.040
33	Dam	28°12′07.70″	26°13′29.52″	6.7	591	0.30	13.08	11.36	14.03	15.50	4.941	37.14	8.120	0.430	0.386	0.016	0.416	0.059	0.215	0.003	0.010
34	Dam	28°12′11.44″	26°13′51.84″	7.3	580	0.31	32.20	1.665	29.94	15.93	2.809	39.10	11.50	0.051	0.029	0.026	0.059	0.014	0.215	0.003	0.010
35	Stream	28°13′28.68″	26°13′15.38″	3.1	593	2.4	3737	7.488	24.90	43.36	14.18	73.60	39.50	16.28	2.910	2.420	28.18	37.96	0.324	1.480	5.220
36	Stream	28°13′16.04″	26°13′27.95″	3.2	711	4.8	5080	0.985	96.24	183.8	14.79	190.2	50.10	22.47	2.910	1.560	5.340	41.12	2.080	2.830	6.740
37	Stream	28°13′16.88″	26°13′06.94″	4.3	580	1.6	3218	0.283	79.21	58.30	9.970	167.4	40.74	5.090	2.910	1.560	0.786	2.687	2.150	0.330	0.380
38	Dam	28°15′07.77″	26°13′10.58″	8.5	574	0.45	47.90	7.368	64.46	39.40	11.22	29.51	7.070	0.053	0.029	0.016	0.008	0.056	0.221	0.033	0.010
39	Dam	28°14′35.78″	26°13′18.17″	8.0	620	0.41	66.29	3.583	46.42	40.49	9.100	27.14	8.670	0.053	0.267	0.016	0.087	0.075	0.221	0.019	0.010
40	Dam	28°14′43.97″	26°14′22.69″	9.1	404	0.39	69.17	4.018	57.18	28.91	8.170	29.12	9.840	0.043	0.896	0.016	0.008	0.075	0.221	0.005	0.010
41	Dam	28°14′12.56″	26°13′59.56″	7.3	612	0.35	29.61	5.798	49.39	35.00	6.120	32.86	9.280	0.149	0.275	0.016	1.235	0.145	0.126	0.003	0.020
42	Dam	28°14′16.93″	26°14′35.35″	6.6	655	0.63	447.1	6.460	22.54	30.00	5.330	24.60	13.06	0.270	0.145	0.012	1.283	2.590	2.076	0.023	0.350
43	Wetland	28°09′56.19″	26°18′19.28″	8.2	112	0.20	19.72	133.0	44.40	33.81	7.110	18.97	4.110	0.090	1.450	0.050	0.050	0.060	0.215	0.010	0.010
44	Wetland	28°10′20.15″	26°20′47.71″	8.5	120	0.16	18.33	144.7	10.76	38.62	6.120	9.910	8.480	0.110	1.950	0.020	0.080	0.140	0.090	0.030	0.010
45	Wetland	28°10′25.19″	26°17′06.55″	7.1	173	0.18	23.04	119.2	56.80	20.95	12.22	22.65	11.33	0.070	1.190	0.040	0.060	0.060	0.170	0.080	0.050
46	Stream	28°08′08.62″	26°16′58.31″	6.2	473	0.66	1429	6.953	35.49	24.19	5.45	81.10	16.18	1.439	0.029	0.189	1.957	8.030	0.221	0.251	0.071
47	Stream	28°08′00.17″	26°16′45.73″	6.9	476	0.69	2906	1.073	17.24	38.81	9.86	106.2	49.53	5.090	2.910	1.560	3.990	0.440	2.150	0.330	0.210

Table 4. Geochemical parameters and chemical composition of ground water samples.

	Location		Field parameters			Major anions			Major cations				Trace elements							
						mg L^{-1}			mg L^{-1}				mg L^{-1}							
Sample No.	E	S	pH	Eh (mV)	EC (mScm^{-1})	SO_4^{2-}	NO_3^-	Cl^-	Na	K	Ca	Mg	Al	Cu	Co	Fe	Mn	Ni	Zn	U
G20	28°07′33.00″	26°13′57.80″	4.9	371	2.69	1015	1.05	20.17	27.1	8.22	18.28	5.480	44.36	10.25	2.06	55.92	12.18	21.60	10.70	0.044
G21	28°06′33.50″	26°13′51.27″	5.7	343	1.01	950.6	4.7	19.22	16.0	6.04	2.66	6.830	6.07	5.82	0.04	39.95	6.44	37.70	6.20	0.039
G26	28°08′08.52″	26°12′53.19″	3.6	380	0.98	2648	4.17	32.64	10.7	10.9	73.60	35.10	0.04	22.30	2.91	9.25	5.06	8.96	0.02	0.162
G27	28°08′06.50″	26°13′00.50″	3.5	314	3.45	3109	2.48	26.95	10.9	14.3	107.2	28.93	0.08	6.80	1.09	15.33	5.678	20.55	0.06	0.095
G28	28°07′58.55″	26°13′07.72″	3.2	363	2.04	2896	16.7	25.81	19.8	13.8	91.40	35.30	0.12	5.52	0.05	4.05	9.081	16.44	0.12	0.082
G29	28°07′44.98″	26°13′16.94″	3.6	382	0.89	2590	23.4	36.87	20.9	45.9	90.70	78.60	7.18	22.86	2.91	33.31	13.45	28.16	2.08	0.08
G30	28°07′41.07″	26°13′41.84″	2.9	390	2.48	3040	15.4	26.38	27.8	28.9	116.5	34.20	18.08	7.96	2.03	17.97	15.09	16.09	21.50	0.125

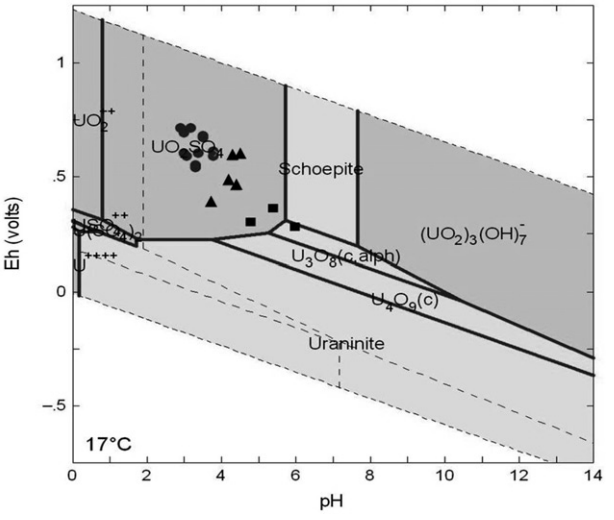

Figure 6. Eh-pH diagram (U-SO_4^{2-}-H_2O system) for uranium speciation in acid mine surface waters with sulphate concentration up to 1000 mg L^{-1}.

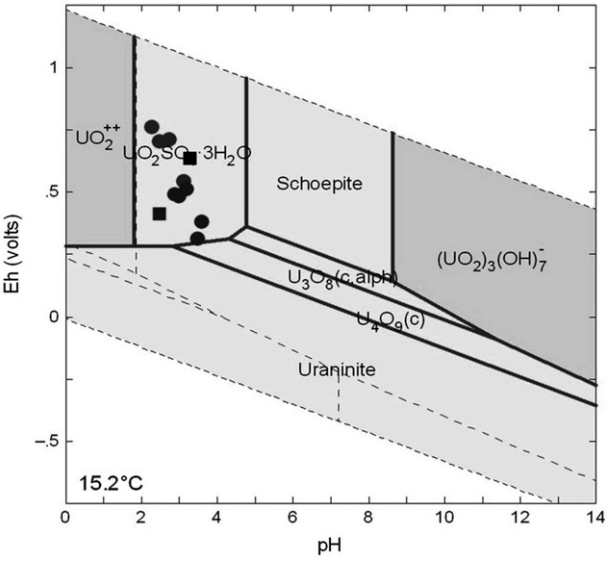

Figure 7. Eh-pH diagram (U-SO_4^{2-}-H_2O system) for uranium speciation in very high sulphate waters with sulphate concentration up to 7000 mg L^{-1}.

that dissolve as others precipitate the model calculates results for the supersaturated system as well as for the system in equilibrium [24].

Case 3 Uranium speciation in pH-buffered sites

The pH buffered sites varied from tailings footprints to streams, wetlands and dams (see Table 3). Liming was done on some tailings footprints to curtail AMD in preparation

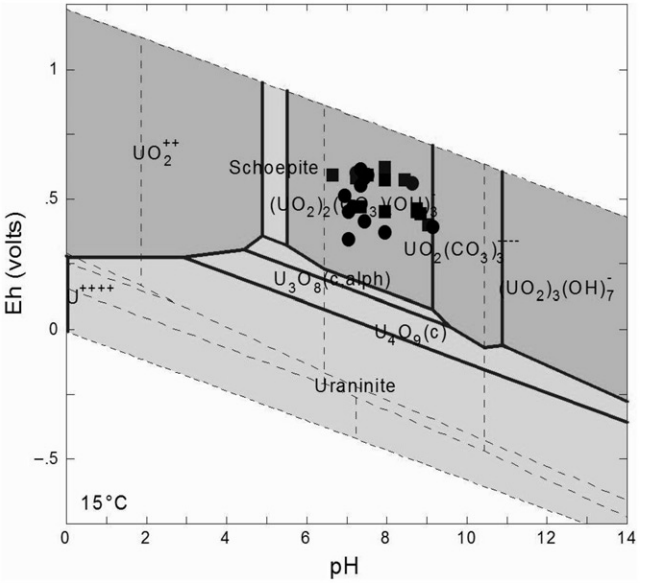

Figure 8. Eh-pH diagram (U-CO_3^{2-}-H_2O system) for uranium speciation in pH-buffered sites.

for rehabilitation. In some streams and dams natural buffering occurs due to the presence of dolomite as well as urban drainage through concrete waterways. Pumping of lime-treated groundwater from mine shafts into some dams by mining companies also leads to pH buffering in the receiving waters.

The model (Figure 8) predicts uranium to exist as the soluble hydroxyl uranyl carbonate complex, $(UO_2)_2(CO_3)(OH)_3^-$ and the uranyl tri-carbonato complex, $(UO(CO_3)_3^{4-}$ (aq)). The model indicates that the addition of lime would not decrease the mobility of uranium except for the very narrow pH range containing schoepite (which indicates hydration). Thus the model predicts uranium to be soluble throughout the whole pH range observed in the field.

The uranyl ion (UO_2^{2+}) forms strong carbonate complexes in most natural waters [7]. Their importance as a function of pH indicates that they largely replace the uranyl-hydroxyl complexes above pH 6 to 11. The carbonate complexes are important because they increase the solubility of uranium minerals, facilitate U(IV) oxidation, and also limit the extent of uranium adsorption in oxidised waters, thus increasing uranium mobility [25].

It is important to note here that while the above cases present inorganic complexing ligand, there is a high influence of organic ligands in the complexation of uranium. The description of the samples in Table 1 reveals a significant presence of organic matter in wetland sediments which could be important for uranium speciation in those environments.

5. Conclusion

Assessment of radioactive disequilibrium in the tailings and wetland sediments has been shown to be a useful tool in assessing the leachability of uranium. The significance of iron

redox speciation on radioactive disequilibrium was also explored. The results showed that iron oxidation and reduction are important when assessing the extent of leachability of uranium in tailings. Radioactive disequilibrium further pointed to some important considerations that should be taken into account, especially when carrying out measurements such as airborne radiometric surveys that are not usually accompanied by 'ground truthing' or direct analyses. Such surveys could yield exaggerated concentrations of uranium in tailings and yet underestimate concentrations in wetlands. This is one reason why such surveys are usually not recommended for geochemical exploration purposes.

The geochemical analyses and modelling of uranium in AMD-impacted sites undertaken through this study provided an improved understanding of the leaching of uranium from tailings dams, and transport of the mobile uranium species through the water systems as complexes of the prevailing ligands in those water systems, e.g. sulphates or carbonates. Uranium then accumulates and becomes enriched in the wetlands downstream of the AMD-impacted areas. Geochemical speciation modelling has been shown to be a useful tool for simulating complex geochemical processes involving contaminant speciation and mobility. This modelling made possible the prediction of many mineral forms in which uranium occurs in the study area. The models predicted that uranium remains soluble in both alkaline and acidic conditions.

Acknowledgements

The authors would like to thank the National Research Foundation for financial support and Mr. A. Kwelilanga of iThemba LABS for technical assistance.

References

[1] D.I. Cole, in *The Mineral Resources of South Africa: Handbook*, edited by M.G.C. Wilson and C.R. Anhausser (Council for Geoscience, Pretoria, South Africa, 1998), Vol. 16, pp. 642–652.
[2] F. Winde and A.B. de Villiers, in *Uranium in the Aquatic Environment*, edited by B.J. Merkel, B. Planer-Friedrich, and C. Wolkersdorfer (Springer-Verlag, Heidelberg, Germany, 2002).
[3] World Nuclear Association (WNA). Available online at: http:www.world-nuclear.org/sym/2005/pdf/Maeda.pdf (accessed 20 August 2008).
[4] F. Winde, presented at the Conference on Environmentally Responsible Mining in Southern Africa, Muldersdrift, Johannesburg, South Africa, 2001 (unpublished).
[5] N.F. Mphephu, Ph.D. thesis, University of the Witwatersrand, 2004.
[6] A.A. Levinson, *Introduction to Exploration Geochemistry*, 2nd ed. (Photopress Inc., Wilmette, IL, USA, 1974).
[7] M. Junghans, D. Degering, C. Helling, and B. Merkel, *Proceedings of the Conference on Uranium Mining and Hydrogeology*, edited by B. Merkel and C. Helling (Freiberg, Germany, 1998), Vol. 2, pp. 216–225.
[8] S. Luo, T.L. Ku, R. Roback, M. Murrell, and T.L. McLing, Geochim. et Cosmochim. Acta **64**, 867 (2000).
[9] M. Ivanovich and R.S. Harmon, *Uranium Series Disequilibrium. Applications to Earth, Marine and Environmental Sciences* (Oxford Science Publications, Clarendon Press, Oxford, 1992).
[10] T.C. Chu, J.J.J. Wang, J. Nucl, and Radiochem. Sciences **1**, 5 (2000).
[11] J. Sato and M.Endo, Japan. J. Nucl. and Radiochem. Sciences **2**, N1 (2001).
[12] US Department of Energy (2004). Available online at: http://www.ocrwm.doe.gov/ymp/index.shtml (accessed 20 May 2006).
[13] F. Winde and L.A. Sandham, Geo. Journal **61**, 131 (2004).

[14] F. Winde, P. Wade, and I.J. van der Walt, Water SA **30**, 219 (2004).
[15] H. Coetzee and H. Szczesniak, presented at the 16th Colloquium of African Geology, Swaziland, 1993 (unpublished).
[16] H. Coetzee, presented at the Symposium on the Application of Geophysics to Environmental and Engineering Problems, Orlando, Florida, USA, 1995 (unpublished).
[17] H. Coetzee, *Proceedings of the Conference on Uranium Mining and Hydrogeology*, edited by B. Merkel and C. Helling (Freiberg, Germany, 1995).
[18] J.W. Funke, Water Research Commission Report, (Pretoria, South Africa, 1990) (unpublished).
[19] H. Tutu, T.S. McCarthy, and E.M. Cukrowska, Applied Geochemistry **23**, 3666 (2008).
[20] H. Tutu, Ph.D. thesis, University of the Witwatersrand, 2006.
[21] H.F. Hermond and E.J. Fechner-Levy, *Chemical Fate and Transport in the Environment* (Academic Press, San Diego, USA, 2000).
[22] M.F. L'Annunziata, editor, *Handbook of Radioactivity Analysis*, 2nd ed. (Academic Press, London, 2003).
[23] S. Clesceri, E. Greenberg, and R. Rhodes, *Standard Methods for the Examination of Water and Waste Water*, 17th ed. (APHA, Washington DC, 1989).
[24] C.M. Bethke, *The Geochemist's WorkbenchTM, Version 2.0, A User's Guide to Rxn, Act2, Tact, React, & Gtplot* (Hydrogeology Program, University of Illinois, 1994).
[25] D. Langmuir, Geochim. et. Cosmochim. Acta **49**, 1931 (1978).